Ga/ZSM-5 Catalyst Improves Hydrocarbon Yields and Increases Alkene Selectivity during Catalytic Fast Pyrolysis of Biomass with Co-fed Hydrogen

Journal:	*Green Chemistry*
Manuscript ID	GC-ART-09-2019-003408.R3
Article Type:	Paper
Date Submitted by the Author:	21-Jan-2020
Complete List of Authors:	Iisa, Kristiina; National Renewable Energy Laboratory, National Bioenergy Center Kim, Yeonjoon; National Renewable Energy Laboratory, Orton, Kellene; National Renewable Energy Laboratory, Robichaud, David; National Renewable Energy Laboratory, Biosciences Center; NREL Katahira, Rui; National renewable Energy Laboratory, Watson, Mike; Johnson Matthey, Technology Centre Wegener, Evan; Argonne National Laboratory, Chemical Sciences and Engineering Division Nimlos, Mark; National Renewable Energy Laboratory, Schaidle, Joshua; National Renewable Energy Laboratory, National Bioenergy Center Mukarakate, Calvin; National Renewable Energy Laboratory, National Bioenergy center Kim, Seonah; National Renewable Energy Laboratory, National Advanced Biofuels Consortium; National Renewable Energy Laboratory, National Bioenergy Center

SCHOLARONE™
Manuscripts

Ga/ZSM-5 Catalyst Improves Hydrocarbon Yields and Increases Alkene Selectivity during Catalytic Fast Pyrolysis of Biomass with Co-fed Hydrogen

Kristiina Iisa[a], Yeonjoon Kim[a], Kellene A. Orton[a], David J. Robichaud[a], Rui Katahira[a], Michael J. Watson[b], Evan C. Wegener[c], Mark R. Nimlos, Joshua A. Schaidle[a], Calvin Mukarakate[*a], and Seonah Kim[*a]

[a]National Renewable Energy Laboratory, 15523 Denver West Parkway, Golden, CO 80401-3393, USA

[b]Johnson Matthey Technology Centre, PO Box 1, Belasis Avenue, Billingham, Cleveland TS23 1LB, UK

[c] Chemical Sciences and Engineering Division, Argonne National Laboratory, 9700 S. Cass Ave., Lemont, Illinois 60439, USA

Corresponding Authors: E-mail: calvin.mukarakate@nrel.gov. Email: seonah.kim@nrel.gov.

Abstract

Catalytic fast pyrolysis using the zeolite ZSM-5 is an attractive process for converting lignocellulosic biomass into fuels and chemicals. Ga-modified ZSM-5 has demonstrated improved hydrocarbon yields compared to ZSM-5 due to additional functionality imparted by Ga; however, there is little knowledge of the active Ga species and its role in the catalytic mechanisms. Here, we employ micropyrolyzer - GC-MS experiments and theoretical calculations to demonstrate that a hydrogen-pretreated Ga species (Ga*/ZSM-5) and a reductive environment are critical towards upgrading pine pyrolysis vapors into high yields of alkenes and aromatic hydrocarbons at near atmospheric pressure. The total carbon yield (g C in product/g C in pine) in alkenes and aromatic hydrocarbons under these conditions was 37% compared to 25% for the parent ZSM-5 catalyst. The corresponding carbon yield was only 19% for Ga*/ZSM-5 under inert conditions indicating that both the hydrogen-pretreated Ga* species and reducing atmosphere are required to obtain high hydrocarbon yields. The ratio of carbon in alkenes to carbon in aromatic hydrocarbons increased to 2.5 with Ga*/ZSM-5 under reductive environment vs. 0.4 for ZSM-5. The carbon yield of alkenes increased with Ga loading; in contrast, increasing catalyst acidity promoted aromatic hydrocarbon production. Experiments conducted with isopropanol demonstrated high selectivity to propene over Ga*/ZSM-5 under reductive environments, indicating enhancement of dehydration reactions. A computational mechanism study was conducted to identify the active Ga species ($[GaH_2]^+$, $[GaO]^+$, $[Ga(OH)_2]^+$ or $[GaH(OH)]^+$) using the dehydration of isopropanol as a model reaction. Theoretical calculations suggested that $[Ga(OH)_2]^+$ and $[GaH(OH)]^+$ are the most likely species responsible for dehydration with 39.7 and 38.8 kcal mol^{-1} activation energy barriers, respectively, and based on thermodynamic analysis, their ratio in the catalyst is dictated by H_2 partial pressure and temperature. The model compound studies and computational results provide mechanistic support for the observed biomass experiments showing increases in alkene selectivity.

1. Introduction

The demand for light alkenes (ethene, propene and butenes), essential building blocks for the chemical industry around the world, is predicted to grow in the future and their supply is currently dependent on petroleum and natural gas production. To close the increasing gap between demand and supply, alternative technologies are being developed to produce alkenes from renewable resources. There is significant ongoing

research on producing alkenes from biomass-derived intermediates such as furan, syngas, methanol, ethanol, butanol and butanediols.[1-4] Catalytic fast pyrolysis (CFP) is an attractive approach for producing alkenes directly from biomass. The majority of reports on biomass CFP using ZSM-5-based catalysts have focused on the production of fuels and aromatic hydrocarbons,[5,6] and a limited number of reports have demonstrated production of phenolic intermediates from aqueous streams.[7, 8] The recovery of coproducts is challenging due in part to the low selectivity of valuable chemicals in CFP oils and the presence of reactive compounds. It is well documented in literature that CFP of biomass conducted in micro to pilot scale reactors using low biomass-to-catalyst ratios produce liquids with a high selectivity to aromatic hydrocarbons, but with low yields of C_2-C_4 alkenes (<10%) except at very high temperatures.[9-14] Anellotech recently demonstrated over 5000 hours of production of high purity *p*-xylene from biomass CFP in their pilot plant and obtained 22-24% liquid yields.[15] While the results from biomass CFP over ZSM-5 are encouraging, there is a need to further improve upon this baseline catalyst to generate alkenes at higher yields.

Doping of ZSM-5 catalysts with various metals has been evaluated for CFP to increase hydrocarbon yields. For example, ZSM-5 modified with nickel and cobalt were evaluated for upgrading beech pyrolysis vapors. The NiO-modified ZSM-5 led to higher yields of aromatic hydrocarbons, and this effect increased with increasing NiO content.[16] Ga has been highlighted in several reports to improve performance of ZSM-5 by enhancing bio-oil or hydrocarbon yields and/or reducing product oxygen content.[17-22] However, other studies did not observe any improvement from Ga-modified ZSM-5.[23,24] This disagreement suggests that specific Ga species may be necessary for improving the catalytic performance of the ZSM-5 material. For instance, extra-framework Ga/ZSM-5 catalysts prepared by ion exchange or incipient wetness methods were found to give a higher selectivity to aromatic hydrocarbons whereas Ga incorporated in the framework decreased catalytic activity compared to unmodified ZSM-5.[18] All of the above-mentioned studies were performed without H_2 pretreatment of the catalysts or the presence of added hydrogen during the catalytic upgrading. There are only limited studies on the impact of H_2-pretreated Ga/ZSM-5 for CFP of biomass. H_2-pretreated Ga/ZSM-5 has

been reported to initially increase dehydrogenation reactions and produce higher aromatics yields during in situ CFP of eucalyptus.[25] For petroleum processes, enhanced aromatics production has been associated with H_2 pretreatment of Ga/ZSM-5 and subsequent oxidation.[5] The H_2 pretreatment converts Ga to a form that can migrate into the interior of ZSM-5 and during the oxidation, the H_2-pretreated Ga is converted to a species more active for aromatization.[26, 27] The exact nature and role of the modified Ga species are not known.

Identifying the active species is critical towards development of new catalysts that exhibit increased yields of fuels and chemicals from biomass CFP.[18, 24] In-situ/operando characterization techniques offer an experimental route to identify the Ga species, but their application to complex reactions such as biomass CFP is challenging. On the other hand, several studies have successfully applied theoretical calculations to evaluate metal-modification of zeolites and elucidate the structures of extra-framework metal dopants during the production of hydrocarbons from model compounds.[28-31] Computational approaches have been used to study catalytic mechanisms in ZSM-5 modified with various metals (Fe,[32-39] Co,[38-40] Cu,[40-42] Zn,[43, 44] Ga,[28, 29, 45-52] and others[31, 53, 54]). Some studies characterized the Ga species using combinations of computational and spectroscopic methods[27, 55-58]. Spectroscopic techniques have identified various Ga species present in zeolites, such as Ga$^+$, gallium hydrides ([GaH$_2$]$^+$, [GaH]$^{2+}$), gallium oxides ([GaO]$^+$, [Ga$_2$O$_2$]$^{2+}$), and gallium hydroxides ([Ga(OH)$_2$]$^+$, [GaH(OH)]$^+$).[27, 55-59] The species observed from spectroscopy have been used in density functional theory (DFT) calculations to evaluate mechanisms of alkane dehydrogenation reactions using Ga/ZSM-5 (see

Table **1**). Computational analysis of free energies can further elucidate the catalytically active species and the corresponding mechanism when multiple possible mechanisms involving two or more species are identified.[28, 29, 45-52] Also, we can gain atomistic insights for designing better catalysts from theoretical investigations; for example, computational phase diagrams unraveled that the state of the metal dopant can be tuned by controlling reaction conditions such as temperature, H_2, and H_2O partial pressures.[58]

These studies have demonstrated that combining experimental and theoretical methods is an effective approach for identifying active Ga species and elucidating their roles in catalysis, especially in industrially relevant processing environments. Despite the synergistic effect of computational and experimental studies, mechanisms for upgrading reactions over $[Ga(OH)_2]^+$ and $[GaH(OH)]^+$ have not been investigated, although they have recently been observed by spectroscopy (Table 1).[58] In addition, the role of Ga species still needs to be elucidated, specifically in terms of enhancing hydrocarbon formation during catalytic upgrading of biomass vapors.

Here, we performed experiments for catalytic upgrading of biomass (pine, cellulose and lignin) pyrolysis vapors over ZSM-5 and Ga-modified ZSM-5 with co-fed H_2 in

a micropyrolyzer - gas chromatograph with a mass spectrometer and a flame ionization detector (py-GC-MS/FID) system and demonstrated that H-pretreated Ga/ZSM-5 produces high yield of alkenes. Compared to ZSM-5, the yield of alkenes increased by more than 200% for experiments conducted with a H-pretreated Ga/ZSM-5 in a reductive atmosphere; however, aromatic hydrocarbons were reduced slightly (~25%). Isopropanol dehydration studies conducted in the same reactor system demonstrated the necessity of both H_2-pretreated Ga species and reductive atmosphere in the production of high yields of propene. Computational studies suggested that both $[Ga(OH)_2]^+$ and $[GaH(OH)]^+$ species may be available in ZSM-5 pores and responsible for enhancing the production of alkenes and overall hydrocarbon yields.

Table 1 Summary of Ga species studied by computational methods for alkane dehydrogenation over Ga-modified zeolites.

Ga species	Summary of computational studies for alkane dehydrogenation	Spectroscopic methods applied for characterization
Ga^+	Enhanced activity when paired with Brønsted acid[29], more active than $[GaH_2]^+$ and $[GaH]^{2+}$ in ethane dehydrogenation[45]	DRIFTS[27, 55], Ga K-edge XANES[56]
$[GaH_2]^+$	Carbanion-like intermediate[28], ethane dehydrogenation – stepwise, isobutane dehydrogenation – concerted[48, 49]	DRIFTS[27, 55], Ga K-edge XANES[56]
$[GaH]^{2+}$	Carbenium-like intermediate[28], enhanced activity when paired with nearby Al sites[46, 47]	DRIFTS[27, 55]
$[GaO]^+$	Very high barrier in catalyst regeneration step[50]	DRIFTS[55], Ga K-edge XANES[56]
$[Ga_2O_2]^{2+}$	Enhanced activity in Ga oxide clusters[52]	Ga K-edge EXAFS[59]
$[Ga(OH)_2]^+$	N/A	Ga K-edge XANES[57, 58] and EXAFS[58]
$[GaH(OH)]^+$	N/A	DRIFTS[55], Ga K-edge XANES and EXAFS[58]

2. Methods

2.1 Materials

Southern yellow pine was supplied by Idaho National Laboratory (INL), Avicel® cellulose was purchased from Sigma Aldrich, and milled wood lignin (MWL) from pine was prepared using the Björkman method.**[60]** The southern yellow pine consisted of 38% cellulose, 25% hemicellulose, and 31% lignin by compositional analysis and the MWL lignin contained 82% lignin. The carbon contents measured using a LECO TruSpec CHN analyzer were 50%, 44%, and 62% for pine, Avicel® cellulose, and MWL lignin, respectively. Parent ZSM-5 catalyst with silica-to-alumina molar

ratio (SAR) of 30 and with 5 wt%, 1 wt%, and 0.5 wt % of Ga were supplied by Johnson Matthey. Ga modification of the parent catalyst was carried out by incipient wetness impregnation using an aqueous solution of gallium nitrate $(Ga(NO_3)_3.6H_2O)$. After impregnation the catalyst samples were dried at 70 °C for 4 hours, 110 °C for a further 4 hours and then calcined at 500 °C for four hours. In addition, Ga/ZSM-5 with SAR 23 and 2.1 wt% and 5.5 wt% Ga was provided by Oak Ridge National Laboratory.

2.2 Catalyst Characterization

The acid site density in the catalysts was measured by transmittance FTIR using self-supported disks of

samples activated at 450 °C in vacuum for 5 hours. The detailed description of this method was given in a previous report.[61] FTIR spectra were collected in the 4000-1200 cm^{-1} spectral range using a Nicolet Protege 460 spectrometer at a 2 cm^{-1} resolution (0.96 cm^{-1} data spacing). An excess of pyridine was admitted into the IR cell at a temperature of 150 °C in a stepwise manner until no changes were observed in the spectra. The saturated sample was then evacuated for 5 min at 150 °C to remove physically adsorbed pyridine and the FTIR spectrum was collected. The spectra were analyzed and presented (including integration, differentiation and determination of peak positions) using specialized Nicolet software, Omnic. Accuracy of the maximum peak positions is estimated to be ±1 cm^{-1} for $\nu_{0\rightarrow1}$ lines, ±2 cm^{-1} for the combination bands and ±5 cm^{-1} for the overtones and some very broad peaks.

Ga K edge XANES measurements were performed on the Material Research Collaboration Access Team (MR-CAT) bending magnet beamline at the Advanced Photon Source, Argonne National Laboratory. The Ga/ZSM-5 sample was ground into a fine powder and pressed into a stainless-steel sample holder forming a self-supporting wafer. The sample holder was sealed in a quartz tube reactor and sealed with two Ultra-Torr fittings with Kapton windows and ball valves through which gases could flow. Prior to hydrogen treatment the sample was dehydrated in flowing helium at 550 °C and a spectrum was acquired at temperature. Following dehydration, the sample was treated with pure hydrogen and a series of spectra were collected at various temperatures: 550 °C, 580 °C, 240 °C, and 150 °C. The XAS data was normalized via standard procedures using the Demeter software suite.[62] The edge energy of each spectrum was determined from the maximum in the first derivative of the XANES.

2.3 Micropyrolysis-GCMS

A tandem micro-furnace pyrolyzer (PY-2020iS, Frontier Laboratories, Japan) coupled to a GC-MS/FID was used to carry out catalytic fast pyrolysis (CFP) experiments. A detailed description of its operation was provided in previous studies.[23, 63] Briefly, this system consists of a pyrolysis zone for generating biomass vapors coupled to a downstream zone for catalytic upgrading. A liquid nitrogen trap placed after the upgrading zone adsorbed the upgraded vapors before they were subsequently desorbed into the inlet of the GC-MS/FID during GC oven heat up. Approximately 500 μg samples of biomass loaded in deactivated stainless-steel cups were automatically dropped into the pyrolysis zone set to 500 °C. The products from the pyrolysis zone were entrained in 54 ml min^{-1} of He carrier gas and passed over a fixed bed of 30 mg catalyst. For experiments conducted in reducing gas atmospheres, 54 ml min^{-1} of H_2 was added prior to the fixed-bed reactor for a total flow of 108 ml min^{-1}. The total pressure was 115 kPa. For each experiment, three successive cups of biomass were passed over the same catalyst bed for a total mass ratio of biomass fed to catalyst of 0.05 g/g. The catalysts were pretreated for 30-60 minutes in either He or a mixture of 50%He/50% H_2. The catalysis zone temperature was varied from 500 to 600 °C. The condensable vapors produced during pyrolysis and upgrading were adsorbed on the liquid nitrogen trap, but light gases such as CH_4 and CO passed through the trap and were separated in a GS-GasPro column and measured by a thermal conductive detector (TCD). The condensable vapors were desorbed from the liquid nitrogen trap and separated in an Ultra-Alloy-5 capillary column, which utilized a stationary phase consisting of 5 % phenyl and 95 % dimethyl polysiloxane. The GC oven was programmed as follows: hold at 40 °C for 3 min then ramp to 240 °C at a rate of 6.0 °C min^{-1}. The separated upgraded species were identified using the NIST GCMS library and quantified based on calibration of twenty compounds representative of upgraded pyrolysis vapors. The carbon yield (g C in compound/g C in feed) was calculated for each product.

Isopropanol dehydration experiments were evaluated in the same py-GC-MS/FID system. Pulses of roughly 0.5 μL of isopropanol were injected into the first reactor, which was set to 250 °C, for volatilization. The resulting vapors were entrained in either He or a mixture of He and H_2 and transported over a catalyst bed of 30 mg as described above for the biomass experiments. Upgrading temperatures of 175-500 °C were investigated, and 250 °C was chosen to reduce the number of competing reactions. Coke formation in the isopropanol experiments was measured by removing the catalyst from the upgrading reactor and determining the mass loss during oxidation of the

catalyst in a thermogravimetric analyzer (TGA) by heating the post-reaction catalyst in air at 20 °C/min from 25 to 780 °C. The mass loss from approximately 250 to 650 °C was attributed to coke while that below 250 °C was attributed to water and weakly adsorbed organic species.[64]

2.4 Computational Details
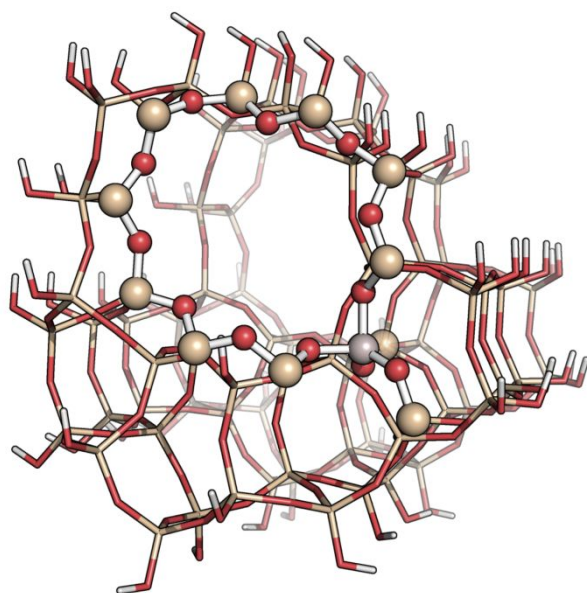
Fig. 1 The model system used in this study. Atoms shown in ball-and-stick representation were treated using DFT and the rest were treated with PM6 method. The Al atom at T12 site is depicted in light purple. For visual clarity, substrate molecules and extra-framework Ga species were omitted in this figure.

A two-layered ONIOM model was used to investigate reactions in Ga/ZSM-5 (Fig. 1).[65] The high level layer which includes an active site and substrate molecules was treated using M06-2X functional[66] with the 6-311G(d,p) basis set. It contains one 10-membered ring (10-MR) having an Al atom at T12 site (most likely site for substitution[67, 68]) and two additional pairs of O-Si atoms connected to the Al. The remaining 295 atoms were included in the low level layer and they were treated with the PM6 semi-empirical method.[69] The atoms in the high level layer were fully relaxed during geometry optimization, whereas others were frozen to maintain crystallographic positions. This model has shown reliable results in a previous mechanism study of ethanol dehydration in HZSM-5.[70] Vibrational frequency calculations were performed for all the reactants, intermediates, products, and transition states (TSs) to verify each state. Intrinsic reaction coordinate (IRC) calculations[71] were also performed for all TSs to locate two minima relevant to each TS. All these calculations were carried out using the Gaussian 09 package,[72] and the GoodVibes program[73] was employed to calculate free energies at an experimental temperature (250 °C) using thermochemistry calculation results from the Gaussian program. Atomic charges of each structure were calculated by natural population analysis (NPA).[74] Surface phase explorer (www.spe.nrel.gov) was used for phase diagram analysis of extra-framework Ga, and its technical details are available in literature. [75]

3. Results and Discussion

3.1 Biomass Vapor Upgrading

Two forms of the 5wt% Ga-modified ZSM-5 were evaluated: one that was pretreated in H_2 for 60 minutes in a flow of 50% He/50% H_2 at 500°C (denoted Ga*/ZSM-5) and one that was pretreated in He only (denoted Ga/ZSM-5). The XANES measurements in Fig. S1 and Table S1 show that the edge energy of the sample in inert atmosphere is at 10.3730 keV, similar to the reported values of isolated Ga^{3+} species on SiO_2 and β-zeolite.[57] Upon hydrogen treatment at 550 °C a shoulder emerges on the leading edge of the spectrum with an inflection point at 10.3695 keV, constituting a decrease in the edge energy of 3.5 eV. When the temperature is increased to 580 °C the shoulder becomes a pronounced peak, still with an inflection point at 10.3695 keV. This observed decrease in edge energy upon hydrogen treatment has been attributed to the formation of low-coordinate Ga^{3+} hydride species[57] and is consistent with the proposed calculated species. Upon cooling to 240 °C the low energy peak decreases in intensity and the edge energy returns to the initial value of 10.3730 keV when the temperature is further decreased to 150 °C.

As shown in Fig. 2a, pine pyrolysis vapors were upgraded over fresh ZSM-5 and 5wt% Ga-modified ZSM-5 (SAR 30) in the tandem micropyrolyzer at low biomass-to-catalyst mass ratios (≈ 0.05 g/g) to produce alkenes, aromatic hydrocarbons, CO and CO_2 in very good agreement with literature data.[18, 23, 63, 76-79] The
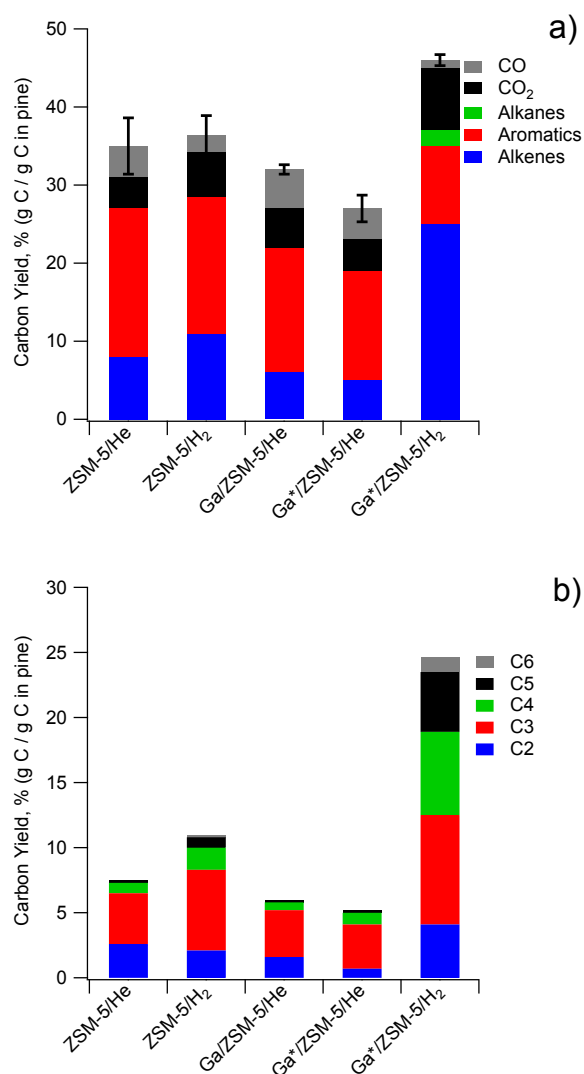
carbon yields for aromatic hydrocarbons were higher than those for alkenes for experiments conducted in He, and they correspond to an alkene-to-aromatic carbon yield ratio of 0.4 g C in alkenes/g C in aromatics. This ratio is similar to previous reports in literature for CFP of woody biomass over ZSM-5.[18, 23] For CFP experiments conducted under inert conditions (He only), the He-pretreated Ga/ZSM-5 and the H_2-pretreated Ga*/ZSM-5 exhibited similar product distributions and alkene-to-aromatic carbon ratios ($\approx$ 0.4) as the unmodified ZSM-5. The yields of the hydrocarbon products were somewhat lower for the Ga-based catalysts than for ZSM-5 due to reduction in the number of Brønsted acid sites caused by the addition of Ga (see Table S2 in the Supporting information) in accordance with several literature results.[80, 81] In contrast, experiments conducted with a H_2-pretreated Ga*/ZSM-5 with cofed H_2 (1:1 He:H_2) (reducing atmosphere) produced significantly higher yields of alkenes and slightly lower yields of aromatic hydrocarbons (**Fig. 2**a) resulting in an alkenes-to-aromatics carbon yield ratio of 2.5. A small fraction of alkanes - methane and some higher alkanes - was also produced. Conducting experiments with Ga*/ZSM-5 under reducing atmosphere increased the carbon yield to hydrocarbons by 48% as compared to ZSM-5 (37% vs. 25%). While the alkene carbon yields for ZSM-5 and for H_2-pretreated Ga*/ZSM-5 in the inert atmosphere (5-8%) are in line with results reported in the literature,[10, 12, 13, 18, 24] the alkene yields for H_2-pretreated Ga*/ZSM-5 under reducing atmosphere, are remarkably high (25%). The results for H_2-pretreated Ga*/ZSM-5 in the inert atmosphere resembled those for non-pretreated Ga/ZSM-5, suggesting that both H_2-pretreated Ga* and continuous H_2 atmosphere are required for the improved hydrocarbon yields. This result suggests that the H_2-pretreated Ga* species was rapidly converted to the non-pretreated form in the absence of hydrogen, as has been reported in the literature.[57, 82] Due to the configuration of the micropyrolyzer, the gas flow through the catalytic reactor was higher in the H_2/He mixture than in He only and, therefore, the contact time was shorter in H_2/He than in He. However, within the experimental error, similar results were obtained for ZSM-5 in both He and 50% H_2/50% He, which suggests that the change in the contact time had little impact on the results.

Carbon oxides were produced in all experiments corresponding to up to 10% carbon yield. The carbon yields of CO and CO_2 were approximately equal in all other experiments except for the one with Ga*/ZSM-5 under reducing atmosphere, which showed a much higher yield of CO_2 than of CO. The reason for this is not clear and may have been due to the difficulty of measuring CO in the presence of high concentrations of H_2. However, one possible explanation is that the H_2-pretreated Ga* species was active for the water gas shift reaction and ZSM-5 and Ga/ZSM-5 were not. The equilibrium constant for the water gas shift reaction is 5 at 500 °C, i.e., H_2 and CO_2 are favored at equilibrium. We estimated the value for the product of $[H_2][CO_2]/[H_2O][CO]$ in the experiments in the He atmosphere based on the production of CO and CO_2 in the experiments, calculated H_2O yield by difference from the oxygen balance, and measured H_2 yield from larger scale CFP experiments over ZSM-5 (0.1% mass yield).[10] The product was over 2 orders of magnitude lower than the equilibrium value, which suggests limited water gas shift activity for ZSM-5 or Ga/ZSM-5 in He. For Ga*/ZSM-5 in the H_2 atmosphere, it is possible that the catalyst converted CO into CO_2 despite the higher bulk H_2 concentration. The water gas shift reaction would also explain the decrease in CO associated with the increase in CO_2 (Fig. *2*a). However, the high yield of CO_2 could also be attributed to decarboxylation reactions catalyzed by Ga*.

The non-detected carbon in these experiments may be attributed to char, coke, and high-boiling compounds not detected by the GC-MS/FID, which could include multiring (3+ rings) polyaromatic hydrocarbons. Char C yield was constant for all experiment at ~40%, and the production of coke and the high-boiling compounds can be approximated by the difference between 60% C yield and the total measured C yield in gases and vapors in Fig. 2a. The results suggest that the yield of coke and high-boiling compounds was reduced for experiments conducted with the Ga*/ZSM-5 in 50% H_2.
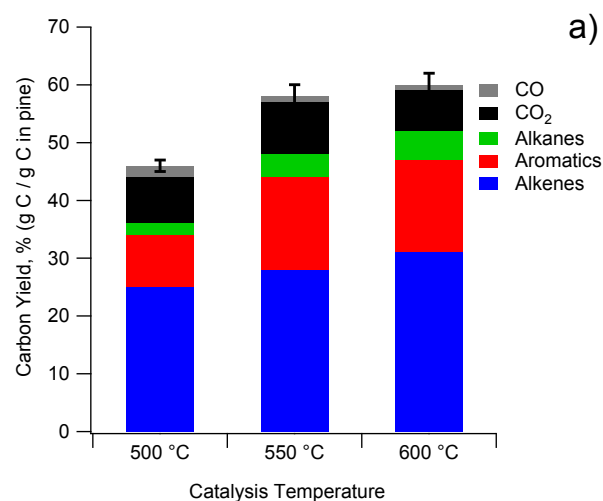
The alkene carbon selectivity data in Fig. 2b shows that H_2-pretreated Ga*/ZSM-5 in 50% H_2 enhanced yield of C_2-C_6 alkenes, but the enhancement was particularly noticeable for higher alkenes (C_{4+}). While ZSM-5, Ga/ZSM-5, and Ga*/ZSM-5 in He produced

mainly C_2 and C_3 alkenes as also reported in the literature,[12, 13, 18, 24] approximately half of the alkenes produced over Ga*/ZSM-5 in 50% H_2 were in the C_{4+} range. The higher alkenes were typically branched, e.g., methylpropene or methylbutene, and included cyclic compounds, e.g., cyclopentene. The increased yield of alkenes is likely due to decreased aromatic yields as shown in Fig. 2a.
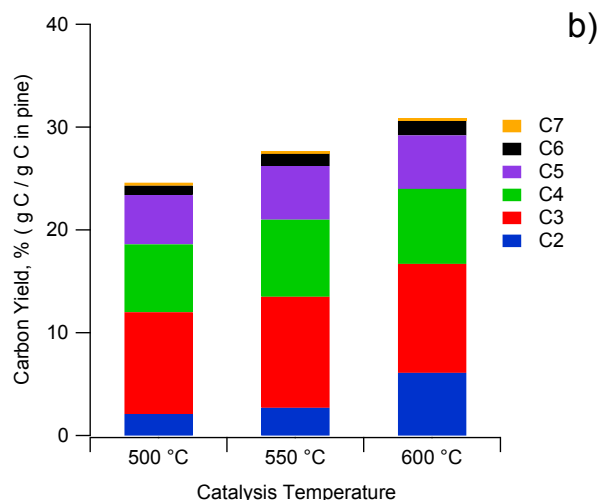
Fig. 3 shows the impact of upgrading temperature on carbon yields and alkene product selectivities during experiments conducted with Ga*/ZSM-5 under reducing atmosphere. Increasing the upgrading temperature enhanced alkene yield, especially of ethene, but had only a modest impact on the yield of higher alkenes. Alkane yield, mostly CH_4, also increased as upgrading temperature increased. ZSM-5 is known to increase alkene and methane yields at higher temperatures,[24, 83] and the observed result is likely due to enhanced cracking activity of ZSM-5 at high temperatures. The aromatic carbon yield also increased as temperature increased from 500 to 550 °C but no further increase was seen as temperature was increased to 600 °C. Aromatics yield over ZSM-5 has a maximum with respect to upgrading temperature;[24, 76, 84, 85] and the peak location is typically reported to be around 600 °C or lower. The results indicate only limited impact of upgrading temperature on the ability of the Ga*/ZSM-5 to form higher alkenes in H_2-containing environments for the range studied.

Fig. 2 Carbon yields in a) light gases and vapors and b) alkenes during upgrading of pine pyrolysis vapors over ZSM-5, non-pretreated 5 wt% Ga/ZSM-5 and H_2-pretreated 5 wt% Ga*/ZSM-5 in either He or 50% H_2/50%He. The values are averages of three successive pulses of biomass over the same catalyst and the error bars reflect the standard deviations of the totals. Reaction conditions: pyrolysis and catalysis performed at 500 °C.

Fig. 3 Carbon yields in a) light gases and vapors and b) alkenes during upgrading of pine pyrolysis vapors over H_2-pretreated Ga*/ZSM-5 in 50% H_2/50% He at different upgrading temperatures. The values are averages of three successive pulses of biomass over the same catalyst and the error bars are the standard deviations for the total yields. Catalysts were tprereated in situ for 30 min at 500 °C in H_2.

A series of Ga*/ZSM-5 catalysts with varying Ga loadings were evaluated in order to gain insight into the role of Ga loading on the observed CFP chemistry (Fig. 4). The previous experiments were performed with a ZSM-5 with SAR of 30 and Ga loading of 5 wt%. The same base catalyst was also loaded with 0.5 wt% and 1 wt% Ga and Table S2 shows that Lewis acid (LA) site density increased with Ga loading, while the Brønsted acid (BA) site density decreased. Another, more acidic ZSM-5 SAR 23 with Ga loadings of 2.1 and 5.5 wt% was also evaluated. Fig. 4 shows that the total alkene carbon yields increased rapidly for Ga loadings up to 1 wt% and then increased more gradually after 1wt% Ga loading. This trend mirrors the plot in Fig. S2 for the ratio of LA-to-BA sites vs. Ga loading, indicating that alkene yield is proportional to the ratio of LA-to-BA sites as this ratio also increases rapidly at low Ga loadings. The carbon yields to aromatic hydrocarbons decreased gradually as the Ga loading increased. A comparison between the results for the catalysts with SAR 30 and 23 showed similar trends as a function of Ga loading, but indicated that increasing catalyst acidity enhanced aromatics yield, as shown by the low alkene-to-aromatics carbon yield ratio for the SAR 23 catalyst. Thus, the catalysts with higher Brønsted acidity (lower SAR) enhanced aromatization, as expected.

CFP experiments using cellulose and lignin were conducted in order to determine the source of the increased alkene yield observed from the studies conducted with Ga*/ZSM-5 in a reductive gas atmosphere. With the control ZSM-5 (SAR 30) and inert conditions, pine, cellulose, and lignin produced roughly similar ratios of alkenes to aromatics (alkenes:aromatics of ~0.5, Fig. 5), with overall hydrocarbon yields higher for cellulose than for lignin. The alkenes-to-aromatics carbon yield ratios agree with calculated values from literature reports for CFP of biopolymers over ZSM-5,[23, 63, 79], which ranged from 0.1 to 0.4 for cellulose and from 0.4 to 0.8 for lignin. The total measured carbon yields for lignin are much lower due to a high carbon loss to char. For the Ga*/ZSM-5 under reducing conditions, cellulose produced much higher hydrocarbon carbon yields (59% vs. 17%) and a higher ratio of alkenes-to-aromatics carbon yields compared to lignin (4.2 vs. 0.9), indicating that most of the alkenes were produced from the carbohydrate component of pine. The alkenes-to-aromatics carbon yield ratio for lignin was only moderately enhanced compared to upgrading over ZSM-5. Fig. 5b also confirmed the formation of C_{4+} alkenes from cellulose. The C_4-C_5 alkene yield for lignin over Ga*/ZSM-5 in H_2 was enhanced compared to that over ZSM-5 as well, and the observed C_{4+} alkenes could possibly be attributed to residual sugars left after lignin extraction from pine. Fig. 5a also shows some alkanes over Ga*/ZSM-5 in the reducing atmosphere. The alkanes were mainly branched, e.g., methylpropane.
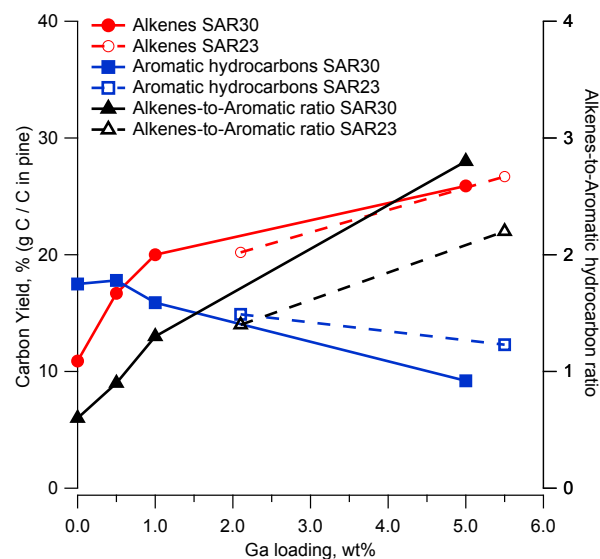
Fig. 4 Carbon yields of alkenes and aromatics, and the carbon yield ratio of alkenes to aromatics during upgrading of pine pyrolysis vapors in 50% H_2/He over H_2-pretreated Ga*/ZSM-5 catalysts with different Ga loadings (0-5.5 wt%) and different SAR values (23 or 30).

The biomass upgrading experiments indicated that C_{4+} alkenes, typically branched alkenes, were formed over Ga*/ZSM-5 in reducing atmosphere. The higher yield of alkenes was coupled with lower aromatic hydrocarbon yields compared to unmodified ZSM-5, Ga/ZSM-5 and Ga*/ZSM-5 for experiments in inert atmospheres. At the same time, the overall yield to hydrocarbons was highest over the Ga*/ZSM-5 in reducing atmospheres. The upgrading over ZSM-5 has been hypothesized to occur via the hydrocarbon pool chemistry in dual cycles of aromatization and alkene interconversions (methylation and cracking)[86] in which aromatics are formed by conversion of higher alkenes originating from the alkene cycle. The results from the current study suggest that the H_2-pretreated Ga* species under reducing environment prevents the aromatization reactions and polycyclic molecular weight growth reactions and formation of coke,[23, 87] which leads to the observed high total hydrocarbon yields.

Several catalytic reaction pathways could contribute to the higher alkene yield. Cellulose was the main source of the higher alkenes over H_2-pretreated Ga*/ZSM-5 in H_2. Alcohol functional groups are prevalent in cellulose and other carbohydrate compounds, and dehydration of the alcohols in biomass pyrolysis vapors is a potential source of the high yields of alkenes. Molecules containing aldehyde, ketone, and acid functional groups are also prevalent in biomass vapors, and we hypothesize that the carbonyl functional groups are initially hydrogenated to alcohols followed by dehydration to stable alkenes, which diffuse out of the ZSM-5 pores without further conversion to aromatics. Our hypothesis for hydrogenation of carbonyls is supported by data in a previous report,[88] which demonstrated a multistep process (low temperature hydrogenation over Ru followed by high temperature hydrogenation over Pt) to convert molecules with carbonyl functional groups present in water soluble bio-oil to produce alcohols for dehydration over zeolites to produce high yields of alkenes and aromatic hydrocarbons (alkene-to-aromatic ratio of 2.3).

In order to gain insight on the production of alkenes from Ga*/ZSM-5 under reductive atmosphere, we conducted experiments and theoretical calculations with isopropanol. Isopropanol was chosen as a model compound because secondary alcohols are pervasive in pyrolysis vapors of cellulose, consisting of levoglucosan and other sugar molecules. An upgrading temperature of 250 °C was used to reduce the number of competing reactions taking place over the catalyst. The goal was to develop mechanisms and reaction pathways to identify chemical transformations occurring on the catalyst sites, provide insight at the atomic scale on why alkenes are produced with H_2-pretreated Ga*/ZSM-5 under reductive atmosphere, and provide data that can be used to develop new catalyst formations for CFP of biomass to produce alkenes.
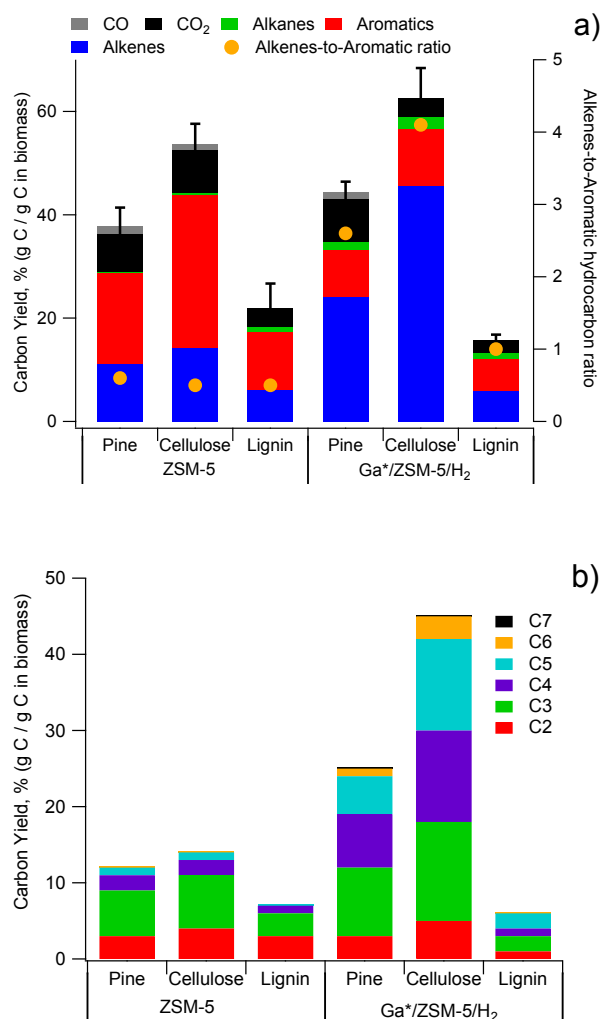
Fig. 5 Carbon yields in a) light gases and vapors and b) alkenes for upgrading of pine, cellulose, and lignin pyrolysis vapors over ZSM-5 in He and over H_2-pretreated Ga*/ZSM-5 in 50% H_2/50% He.

3.2 Dehydration of Isopropanol

To investigate dehydration reactions and the effect of the H_2 pretreatment of Ga, isopropanol upgrading experiments were conducted in the py-GC-MS/FID system using ZSM-5, Ga/ZSM-5, and Ga*/ZSM-5 under either inert or reducing atmosphere. Fig. 6a shows that propene was the main product from Ga*/ZSM-5 in 50% H_2. The selectivity to propene was 66%, and minor amounts of higher alkanes or alkenes (<10% conversion) were also formed. This contrasts with ZSM-5, which produced a mixture of alkanes and alkenes. The alkanes from ZSM-5 were mainly in the range of C_4-C_7 but with compounds up to C_{11} detected, and the alkenes were mainly in the range of C_3-C_7.

Both alkanes and alkenes consisted to a large extent of branched compounds, e.g., methylpropane and methylpropene, and methylbutanes and methylbutenes. Ga/ZSM-5 produced similar product distributions as ZSM-5 did. The product distributions from ZSM-5 and Ga/ZSM-5 were similar regardless of whether the experiments were conducted in reducing or inert atmospheres (Fig. 6b).
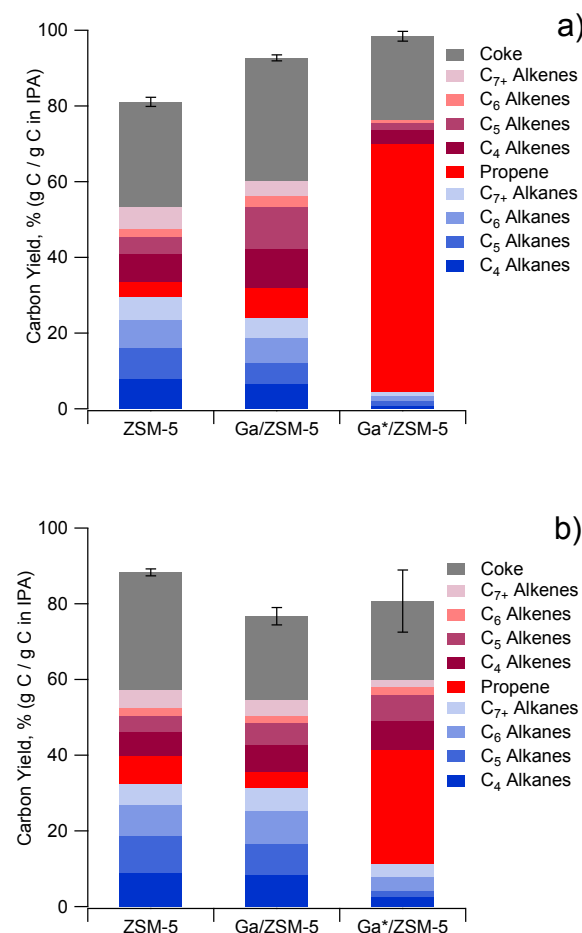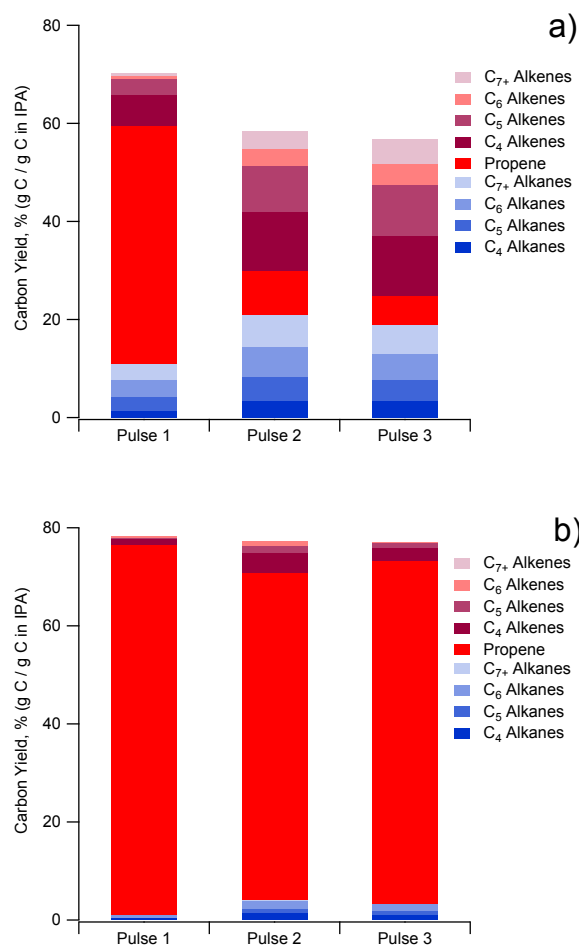

Fig. 6 Upgrading of isopropanol over ZSM-5, non-pretreated Ga/ZSM-5 and H_2-pretreated Ga*/ZSM-5 in a) 50% H_2/50% He and b) He only at 250°C. The results are averages of three pulses of isopropanol passed over the same catalyst bed; the error bars reflect the standard deviation for the total amount of gas and vapor products.

Propene was the predominant product over Ga*/ZSM-5 (Fig. 6), which suggests that the H_2-pretreated Ga* species promoted the formation of molecular propene from dehydration of isopropanol. In contrast, longer chain alkenes and alkanes were formed over ZSM-5 and Ga/ZSM-5 in addition to small amounts of

propene. This suggests that direct dehydration of isopropanol to molecular propene and diffusion of propene out of the catalyst pores was not the dominant reaction, but isopropanol, propene, or other intermediates remained adsorbed on the catalytic sites and were converted to a variety of other compounds. It has been postulated that surface alkoxy species can be formed on zeolite surfaces (Brønsted acid sites) via dehydration of alcohols, e.g., methoxy from methanol and analogously iso-propoxy from isopropanol.[89] The H_2-pretreated Ga* may enable rapid H transfer to the surface oxygen with reformation of the Brønsted acid site and release of propene before it has time to react further. This is possible due to enhanced catalytic activity of H_2-pretreated Ga* species in C-H activation; details of which will be discussed in the following computational section. In the absence of H_2-pretreated Ga*, it is proposed that the iso-propoxy species remains on the surface longer and has time to further react via reactions similar to those in the alkyl interconversion cycle with methanol in MTG and MTO (methanol-to gasoline and methanol-to-olefins) processes.[86] It should be noted that the formation of propene from isopropanol is distinctly different from the MTO process since it represents direct dehydration of an alcohol to alkene as opposed to an increase in the carbon number from the alcohol (methanol) to the alkenes (C_{2+}) in the MTO process. The fact that light hydrocarbons with carbon numbers of 4-7 were all formed in relatively similar proportions over ZSM-5 and non-pretreated Ga/ZSM-5 suggests that scission of C-C bonds of the isopropanol or its derivatives was important. Without C-C scission, the product would have been composed of only C_3, C_6, C_9, etc., hydrocarbons. The alkenes started from C_3, suggesting some direct dehydration of isopropanol, whereas the alkanes started from C_4, suggesting that they were formed from reactions of the isopropanol intermediate and a hydrocarbon fragment. Both alkanes and alkenes were identified by the GC-MS. The mechanism for alkane formation is not known but higher alkane yield has been previously reported for CFP over Ni/ZSM-5[16].

Interestingly, the Ga*/ZSM-5 under inert atmosphere (Fig. 6b) gave a product with a yield between that of H_2-pretreated Ga*/ZSM-5 in H_2 and those of the other experiments, consisting of approximately 30% propene and significant proportions of both higher alkanes and alkenes. It is important to note that the results given in Fig. 6 are averages of three consecutive injections of isopropanol. To gain more insight on the data from Ga*/ZSM-5 in inert atmosphere, an analysis of the individual pulses in Fig. 7a shows that the first pulse produced predominantly propene, but the later pulses gave product distributions similar to those of ZSM-5 and Ga*/ZSM-5. This change in product selectivity is in accordance with an initial presence of H_2-pretreated Ga in the catalyst and rapid conversion of the H_2-pretreated form of Ga to the non-pretreated form (Fig. S1) as reported in the literature.[82] Fig. 7b shows that the high propylene selectivity was maintained with H_2-pretreated Ga* under reductive environment. Coke was formed in relatively similar quantities over all catalysts (Fig. 6), which suggests that the change in selectivity was not due to coke formation. During the tandem reactor experiments, there is a time lapse of approximately 30 minutes between each pulse of biomass due to the time required to complete the GC-MS analysis. During this time, the reaction gas flows continuously through the catalyst bed. To test if the absence of hydrogen during this time could convert the H_2-pretreated Ga* to the non-pretreated form or if a flow of an oxygenated compound (here isopropanol) was required, an experiment was performed in which 60 minutes was elapsed before a pulse of isopropanol was injected. The experiment showed a product distribution more resembling that of Ga/ZSM-5. This indicates that the H_2-pretreated Ga* is converted to the non-pretreated form if H_2 is removed from the feed gas. In contrast, no increased yield of propene was detected in later pulses of isopropanol for Ga/ZSM-5, indicating that the non-pretreated Ga was not easily converted to the H_2-pretreated form at this reaction temperature. No CO or CO_2 was detected over any catalyst, which indicates that dehydration or hydrodeoxygenation was the predominant deoxygenation reaction. The amount of coke on the catalyst was quantified after each set of three isopropanol pulses, and 20-30% of the carbon in the isopropanol was converted to coke in these experiments. Coke yield appeared to be slightly lower for the H_2-pretreated Ga*/ZSM-5 in H_2. However, there was a high uncertainty in the coke measurement due to the small mass of the catalyst samples and difficulty in collecting the post-reaction catalyst quantitatively. Coke formation will be investigated in more detail in our future work.

Fig. 7 Analysis of individual pulses for upgrading of isopropanol over H_2-pretreated Ga*/ZSM-5 at 250 °C in, a) He only and B) 50% H_2/50% He.

## 3.3 Computational Calculations for Identifying Active Species

Based on literature results,[28, 46-49, 56-58] we selected four Ga species, $[GaH_2]^+$, $[GaO]^+$, $[Ga(OH)_2]^+$, and $[GaH(OH)]^+$, as possible species present in ZSM-5

under reducing conditions and responsible for the observed increase in alkene yields.[27, 55-58] Theoretical calculations were conducted to identify which Ga active species is the most likely active form for dehydration of isopropanol.

3.3.1. Isopropanol dehydration on $[GaH_2]^+$. $[GaH_2]^+$ can be considered as one of the H_2-pretreated forms of extra- framework Ga. Fig. 8 illustrates the proposed reaction mechanism for isopropanol dehydration using $[GaH_2]^+$ reactive species, and the calculated free energy surface at 250 °C. The reaction is initiated by adsorption of isopropanol onto the Ga site ($R_{ads}\_[GaH_2]^+$). The adsorption is exothermic with 14.1 kcal mol^{-1} stabilization in free energy which accompanies formation of the Ga-O(H) bond and the hydrogen bond between the hydroxyl group of the reactant and the framework oxygen (1.51 Å). Then C-H activation at β-carbon (β-C) of the reactant is followed via the $TS1\_[GaH_2]^+$, giving rise to the intermediate $IM1\_[GaH_2]^+$; the hydrogen at β-C is migrated to the framework oxygen to form the Ga-β-C bond. The free energy activation barrier ($\Delta G^{\ddagger}$) of this reaction is 50.2 kcal mol^{-1}. Afterwards, the dehydration takes place by passing through the $TS2\_[GaH_2]^+$, for which $\Delta G^{\ddagger}$ is 8.1 kcal mol^{-1}, to yield the propene and H_2O product complex, $P\_[GaH_2]^+$. This reaction involves dissociation of the Ga-β-C bond and the hydroxyl group to form propene, and formation of the H_2O via the dissociated OH group from isopropanol and the H from framework O. The rate-determining step (RDS) of the reaction, based on the highest calculated activation energy, is the C-H bond activation ($R_{ads}\_[GaH_2]^+ \rightarrow TS1\_[GaH_2]^+$), with $\Delta G^{\ddagger}$ of 50.2 kcal mol^{-1}. It is unlikely that this step proceeds at a competitive rate given the reaction temperature.
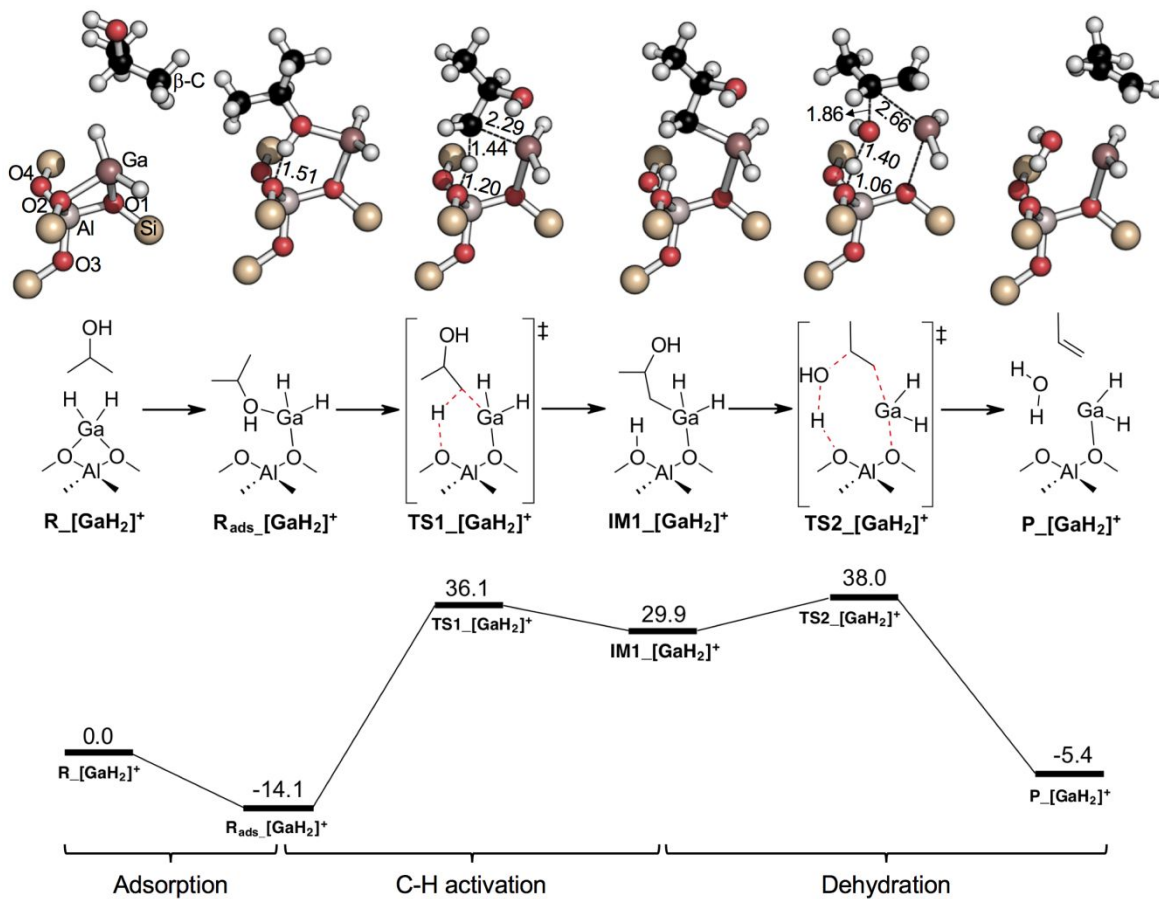
Fig. 8 Gibbs free energy diagram for the isopropanol dehydration on [GaH$_2$]$^+$ (bottom) with reaction mechanism (middle) and calculate geometries (top). For clear representation of reactions, only the key part in QM region is shown in top row. The calculations were conducted using the ONIOM (M06-2X/6-311G(d,p):PM6) model at 250 °C. All the Gibbs free energy values are in kcal mol^{-1}.
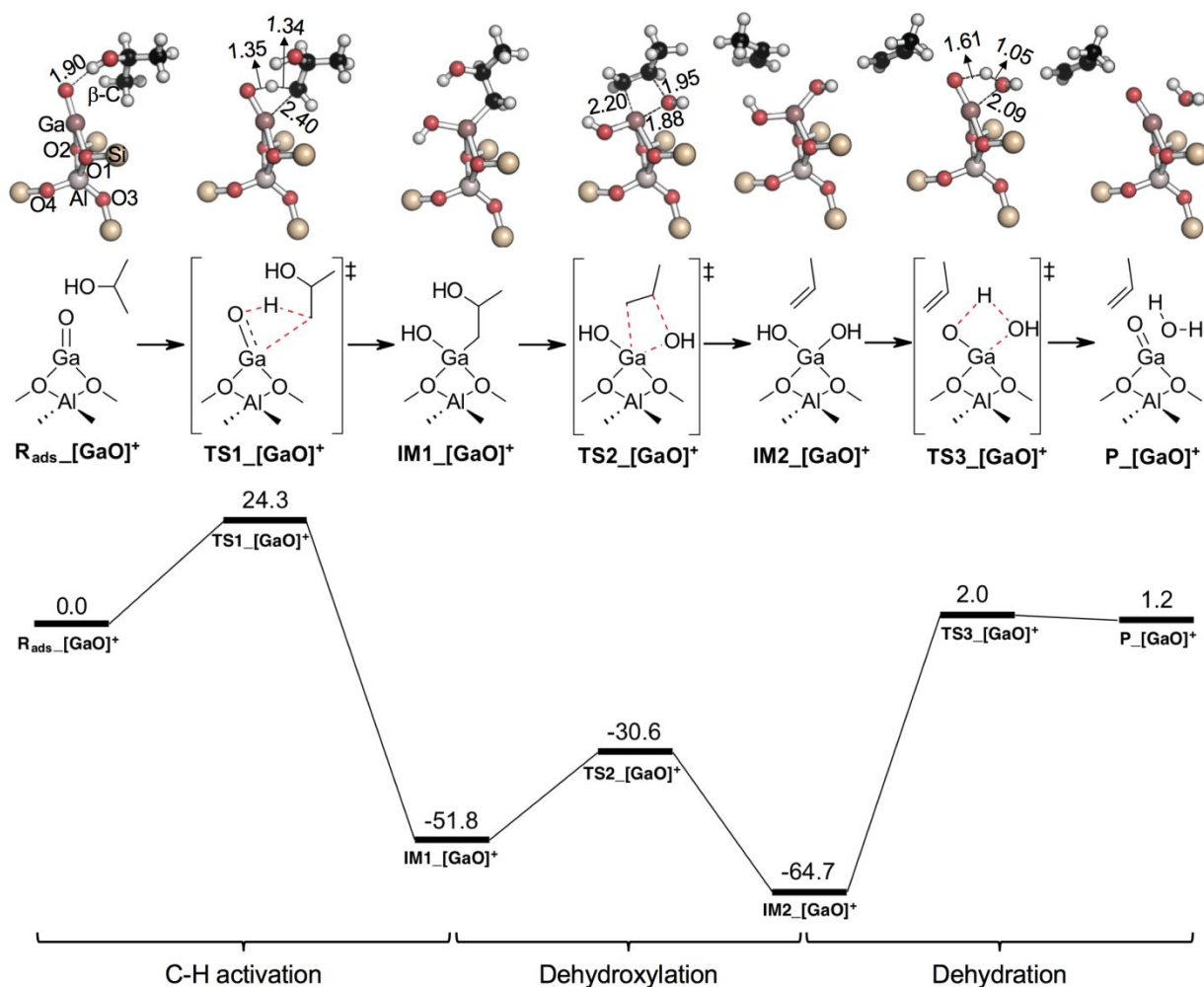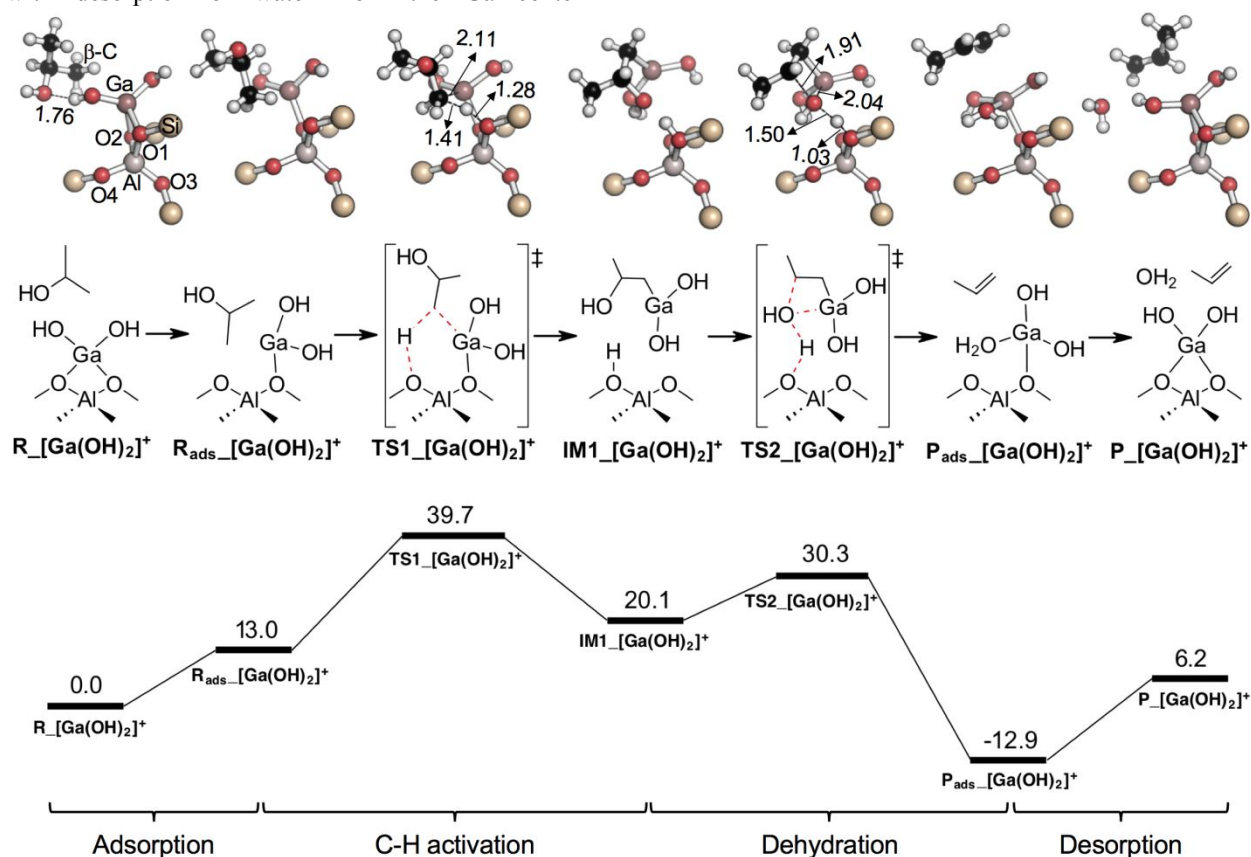
Fig. 9 Gibbs free energy diagram for the isopropanol dehydration on $[GaO]^+$ (bottom) with reaction mechanism (middle) and calculate geometries (top). For clear representation of reactions, only the key part in QM region is shown in top row. The calculations were conducted using the ONIOM (M06-2X/6-311G(d,p):PM6) model at 250 °C. All the Gibbs free energy values are in kcal mol^{-1}.

3.3.2. Isopropanol dehydration on $[GaO]^+$. Reaction energetics with $[GaO]^+$ as an active non-pretreated Ga species was calculated and is shown in Fig. 9. The reaction starts with **R_{ads}_$[GaO]^+$** which is formed via a hydrogen bond with the Gallyl oxygen (1.90 Å). Next, it undergoes C-H activation which leads to hydrogen transfer from the β-C to the oxygen bound to $[GaO]^+$ and Ga-β-C bond formation (**IM1_$[GaO]^+$**) through **TS1_$[GaO]^+$**. The subsequent reaction step results in the propene product through migration of the hydroxyl group from the substrate to the Ga center (**IM2_$[GaO]^+$**) via **TS2_$[GaO]^+$**. These two steps result in transformation of the $[GaO]^+$ extra-framework into the $[Ga(OH)_2]^+$ reactive species. ΔG‡

of these two steps are 24.3 and 21.2 kcal mol^{-1}, respectively.

For regeneration of the catalytic cycle of the $[GaO]^+$ reactive species, the dehydration reaction is followed by conversion of the **IM2_$[GaO]^+$** via the **TS3_$[GaO]^+$** with ΔG‡ of 66.7 kcal mol^{-1}. The barrier for the regeneration step is higher than that for the RDS of $[GaH_2]^+$ (50.2 kcal mol^{-1}), indicating that $[GaO]^+$ is also catalytically inactive in terms of reaction kinetics. Our result is also consistent with a previous computational study for $[GaO]^+$, which reported that the catalyst regeneration step in alkane dehydrogenation is not kinetically feasible.[50]
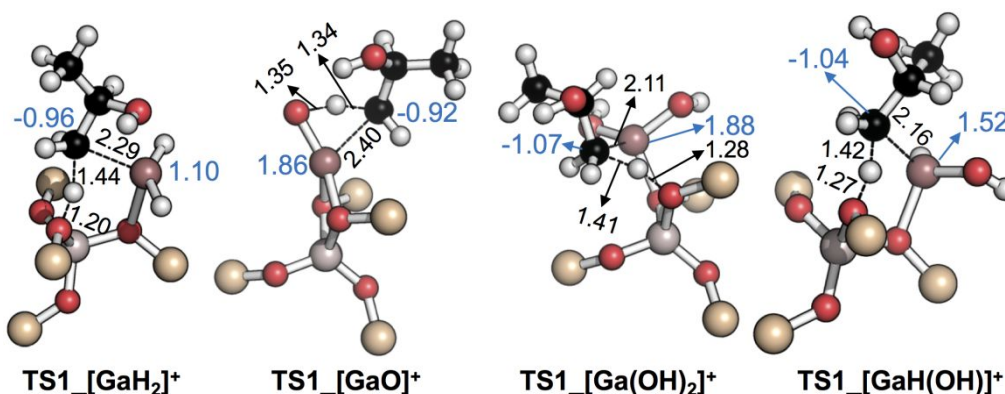
3.3.3. Isopropanol dehydration on [Ga(OH)₂]⁺. Fig. 10 illustrates the free energy surface of isopropanol dehydration over [Ga(OH)₂]⁺, which was observed as a stable Ga complex in Fig. 9 (**IM2_[GaO]⁺**), and also in recent spectroscopic studies.[68,69] The reactant is adsorbed (**R_ads_[Ga(OH)₂]⁺**) and the β-C-H bond is activated through the **TS1_[Ga(OH)₂]⁺** with ΔG‡ of 39.7 kcal mol⁻¹. It generates the **IM1_[Ga(OH)₂]⁺** through hydrogen migration to the framework oxygen (O1) and Ga-β-C bond formation. After the C-H activation, the propene is readily formed (**P_ads_[Ga(OH)₂]⁺**) by passing through the dehydration TS (**TS2_[Ga(OH)₂]⁺**) with ΔG‡ of 10.2 kcal mol⁻¹. The catalytic cycle is finally completed with desorption of water from the Ga center

(**P_[Ga(OH)₂]⁺**). The [Ga(OH)₂]⁺ reactive species exhibited a lower ΔG‡ for the RDS (39.7 kcal mol⁻¹) as compared to the other Ga species such as [GaH₂]⁺ (50.2 kcal mol⁻¹) and [GaO]⁺ (66.7 kcal mol⁻¹), which suggests that [Ga(OH)₂]⁺ is one of the active forms of extra-framework Ga in ZSM-5 in terms of reaction kinetics.

Fig. 10 Gibbs free energy diagram for the isopropanol dehydration on [Ga(OH)₂]⁺ (bottom) with reaction mechanism (middle) and calculate geometries (top). For clear representation of reactions, only the key part in QM region is shown in top row. The calculations were conducted using the ONIOM (M06-2X/6-311G(d,p):PM6) model at 250 °C. All the Gibbs free energy values are in kcal mol⁻¹.

Fig. 11 Optimized structures of transition states of C-H activation step for $[GaH_2]^+$, $[GaO]^+$, $[Ga(OH)_2]^+$, and $[GaH(OH)]^+$ with bond distances (black, in Å) and NPA charges (blue).

3.3.4. Isopropanol dehydration on $[GaH(OH)]^+$. Another possible candidate for the extra-framework Ga is $[GaH(OH)]^+$, whose presence was also suggested under reducing conditions.[58] Reaction kinetics of $[GaH(OH)]^+$ were scrutinized and Fig. S3 shows the calculated free energy surface of the reaction. It necessarily follows similar reaction pathways as those for $[Ga(OH)_2]^+$, and the RDS of the $[GaH(OH)]^+$ is the C-H activation, with $\Delta G^{\ddagger}$ of 38.8 kcal mol^{-1} (**TS1_$[GaH(OH)]^+$** in Fig. S3. This activation barrier is 0.9 kcal mol^{-1} lower than that for $[Ga(OH)_2]^+$, which suggests that $[GaH(OH)]^+$ is another active form of Ga. The presence of these active forms in the reducing experimental conditions was also verified by phase diagram analysis (*vide infra*).

3.4 Role of Ga in stabilizing C-H activation transition states.

It is also of importance to analyze the C-H activation step because, for all four of the reactive Ga species studied, C-H activation has the highest $\Delta G^{\ddagger}$ among the reaction steps occurring until propene formation. In other words, stabilization of the TS by the electrostatic interaction between Ga and β-C is crucial for reactions to take place with low activation energy. To compare Ga-β-C interactions of the C-H activation TSs for different Ga species, atomic charges of Ga (Q_{Ga}) and β-C ($Q_{\beta-C}$) were calculated by NPA,[74] and Ga-β-C bond distances ($D_{Ga-\beta-C}$) were also measured.

Fig. 11 shows the geometries, NPA charges, and characteristic bond distances of C-H activation TSs.

$Q_{\beta-C}$ values are negative for all the four Ga species: -0.96, -0.92, -1.07, and -1.04 for $[GaH_2]^+$, $[GaO]^+$, $[Ga(OH)_2]^+$, and $[GaH(OH)]^+$, respectively. The carbanionic β-C should be stabilized by closer interaction with a more electropositive Ga center (i.e., lower $D_{Ga-\beta-C}$ with highly positive Q_{Ga}), which leads to more viable C-H activation. In terms of Q_{Ga} values, $[GaO]^+$ (1.86) and $[Ga(OH)_2]^+$ (1.88) have a more positive charge than $[GaH(OH)]^+$ (1.52) does, while $[GaH_2]^+$ has the least positive Ga center (1.10). The β-C of $[Ga(OH)_2]^+$ and $[GaH(OH)]^+$ has closer interaction ($D_{Ga-\beta-C}$ = 2.11 and 2.16 Å, respectively) than that for $[GaH_2]^+$ (2.29 Å), whereas $[GaO]^+$ showed the farthest Ga-β-C distance (2.40 Å). The electrostatic interaction between the Ga and β-C is proportional to the Coulomb force $Q_{Ga}Q_{\beta-C}/(D_{Ga-\beta-C})^2$; the magnitude of the force in atomic unit follows the order $[Ga(OH)_2]^+$ (0.13) > $[GaH(OH)]^+$ (0.10) > $[GaO]^+$ (0.08) > $[GaH_2]^+$ (0.06). This is consistent with the kinetic analysis discussed in the previous sections, which demonstrated that isopropanol dehydration is kinetically more favorable for $[Ga(OH)_2]^+$ and $[GaH(OH)]^+$ than for $[GaO]^+$ and $[GaH_2]^+$. The aforementioned analysis of reaction energetics and TS structures determined the favorable Ga species in terms of reaction kinetics; however, it should be further corroborated that these species exist under the given experimental conditions. To this end, we conducted phase diagram analysis as discussed in the next section.

3.5 Identifying the active forms of Ga* under experimental conditions

To provide guidance for future catalyst design, it is critical that the active form(s) of Ga in the Ga*/ZSM-5 catalyst under reducing conditions, which showed the highest alkene yield (Fig. 2a), is identified. For this purpose, energetics of transformations among all four extra-framework Ga species studied were investigated, and the phase diagram of Ga active species was obtained with respect to different reaction conditions.[75] Fig. S4 shows the presence of different Ga species as a function of H_2 partial pressure and temperature at a fixed water partial pressure of 10^{-6} bar. Either $[GaH(OH)]^+$ or $[GaH_2]^+$ is present at the reaction conditions for the biomass upgrading (denoted by the blue box in Fig. S4). The former showed the lowest $\Delta G^{\ddagger}$ of RDS (38.8 kcal mol^{-1}, Fig. S3), and at higher temperature, the latter can also be responsible for the catalysis, considering the RDS barrier of 50.2 kcal mol^{-1} (Fig. 8). On the other hand, the red square in Fig. S4 denotes the reaction conditions for upgrading of isopropanol. In this region, the Ga species predominantly exists as either $[Ga(OH)_2]^+$ or $[GaH(OH)]^+$ which are both kinetically desirable in terms of $\Delta G^{\ddagger}$ of RDS. All these results are in line with the experiments for both biomass and isopropanol, which showed higher alkene yield in the presence of H_2 (Ga*/ZSM-5/H_2 in Fig. 2a and Ga*/ZSM-5 in Fig. 6a). The effect of water pressure on active forms of Ga* was also investigated; under higher water concentrations (0.01 bar) the phase transitions shift such that $[Ga(OH)_2]^+$ is more dominant under the experimental conditions of this work (Fig. S5).

3.6 Role of Ga* in enhancing alkene selectivity

To maximize alkene selectivity, the Ga* species should prevent further reactions of alkenes such as aromatization. Fig. 4 shows that increasing Ga loading results in lower yields of aromatics during catalytic upgrading of pine pyrolysis vapors. This result is also in line with that of isopropanol upgrading shown in Fig. 6a; the Ga*/ZSM-5 showed less yield of C_6, C_{7+} alkanes and alkenes, products from oligomerization of propene, than ZSM-5. This indicates that the Ga*/ZSM-5 inhibits aromatization, which is followed by oligomerization reactions, and thus increases alkene selectivity. To elucidate the role of Ga*, computational mechanism study was conducted for propene oligomerization into 1-hexene (C6 alkenes). Fig. S6 illustrates the proposed mechanisms and their energetics for two active Ga* species ($[Ga(OH)_2]^+$ and $[GaH(OH)]^+$). The two species follow the similar pathway for oligomerization (Figs. S6a and S6b). The oligomerization over $[Ga(OH)_2]^+$ (64.9 kcal mol^{-1}) and $[GaH(OH)]^+$ (61.7 kcal mol^{-1}) showed higher $\Delta G^{\ddagger}$ than dehydration (39.7 and 38.8 kcal mol^{-1} for $[Ga(OH)_2]^+$ and $[GaH(OH)]^+$, respectively), due to the steric hindrance around the Ga center and zeolite pores. This is consistent with the enhancement of propene yield in Ga*/ZSM-5 by suppressing subsequent reactions after dehydration of isopropanol into propene.

4. Conclusion

An integrated experimental and theoretical investigation was conducted to understand the role of Ga addition to ZSM-5 on catalytic fast pyrolysis of biomass. The experiments showed that a H_2-pretreated Ga species and reductive environments are critical towards production of high yields of hydrocarbons during CFP of biomass at near atmospheric pressures. The H_2-pretreated Ga species enhances production of alkenes; in contrast, ZSM-5 acidity favors coupling and cyclization of alkenes to form aromatic hydrocarbons. Increasing Ga loading improves alkene production. Alkenes are favorably produced from the carbohydrate (cellulose) component of pine. Experiments conducted with isopropanol confirmed that H_2-pretreated Ga/ZSM-5 in H_2 atmosphere enhances the selectivity of the dehydration product, propene. To identify the kinetically active form of Ga species, theoretical calculations were performed using isopropanol as a model compound; they suggested that $[Ga(OH)_2]^+$ and $[GaH(OH)]^+$ are the most likely active catalytic sites responsible for dehydration of isopropanol. However, their presence in H_2-pretreated Ga/ZSM-5 still needs to be confirmed experimentally through spectroscopic studies. Analysis of the computed Ga phase diagram suggested that these two species also mainly exist in our isopropanol dehydration experimental conditions in the presence of H_2. To the best of our knowledge, this is a first-of-its-kind study utilizing experiments with whole

biomass vapors, theory, and model compounds to identify reactive species in complex catalytic fast pyrolysis reaction environments. These findings provide both experimental and mechanistic insight into the biomass deoxygenation reaction which can be utilized in the systematic development of the catalytic process with higher hydrocarbon yield.

Conflicts of interest

There are no conflicts to declare

Acknowledgement

References

1. V. Zacharopoulou and A. Lemonidou, *Catalysts*, 2018, **8**, 2.
2. F. Cavani, S. Albonetti, F. Basile and A. Gandini, *Chemicals and Fuels from Bio-Based Building Blocks*, 2016Wiley-VCH Verlag GmbH & Co. KGaA, 1st edn., 2016.
3. H. M. Torres Galvis and K. P. de Jong, *ACS Catal.*, 2013, **3**, 2130-2149.
4. Y.-T. Cheng and G. W. Huber, *ACS Catal.*, 2011, **1**, 611-628.
5. C. M. Lok, J. Van Doorn and G. Aranda Almansa, *Renew. Sust. Energ. Rev.*, 2019, **113**, 109248.
6. A. Heeres, N. Schenk, I. Muizebelt, R. Blees, B. De Waele, A. J. Zeeuw, N. Meyer, R. Carr, E. Wilbers and H. J. Heeres, *ACS Sust. Chem. Eng.*, 2018, **6**, 3472-3480.
7. A. N. Wilson, M. J. Price, C. Mukarakate, R. Katahira, M. B. Griffin, J. R. Dorgan, J. Olstad, K. A. Magrini and M. R. Nimlos, *ACS Sust. Chem. Eng.*, 2017, **5**, 6615-6625.
8. A. N. Wilson, A. Dutta, B. A. Black, C. Mukarakate, K. Magrini, J. A. Schaidle, W. E. Michener, G. T. Beckham and M. R. Nimlos, *Green Chem.*, 2019, **21**, 4217-4230.
9. K. Iisa, R. J. French, K. A. Orton, A. Dutta and J. A. Schaidle, *Fuel*, 2017, **207**, 413-422.
10. K. Iisa, R. J. French, K. A. Orton, M. M. Yung, D. K. Johnson, J. ten Dam, M. J. Watson and M. R. Nimlos, *Energy & Fuels*, 2016, **30**, 2144-2157.
11. C. Mukarakate, X. D. Zhang, A. R. Stanton, D. J. Robichaud, P. N. Ciesielski, K. Malhotra, B. S. Donohoe, E. Gjersing, R. J. Evans, D. S. Heroux, R. Richards, K. Iisa and M. R. Nimlos, *Green Chem.*, 2014, **16**, 1444-1461.
12. V. Paasikallio, K. Kalogiannis, A. Lappas, J. Lehto and J. Lehtonen, *Energy Technol.*, 2017, **5**, 94-103.
13. K. Wang, P. A. Johnston and R. C. Brown, *Bioresource Technology*, 2014, **173**, 124-131.
14. K. Wang, K. H. Kim and R. C. Brown, *Green Chem.*, 2014, **16**, 727-735.
15. Anellotech pilot plant campaign surpasses 5,000 hours of operations, achieving both yield and reactor outlet oxygenate targets,

https://www.anellotech.com/news-1, (accessed Jul. 26th, 2019).

16. E. F. Iliopoulou, S. D. Stefanidis, K. G. Kalogiannis, A. Delimitis, A. A. Lappas and K. S. Triantafyllidis, *Appl. Catal. B*, 2012, **127**, 281-290.

17. H. J. Park, Y.-K. Park, J.-S. Kim, J.-K. Jeon, K.-S. Yoo, J.-H. Yim, J. Jung and J. M. Sohn, in *Studies in Surface Science and Catalysis*, 2006, vol. 159, p. 553.

18. Y. T. Cheng, J. Jae, J. Shi, W. Fan and G. W. Huber, *Angewandte Chemie*, 2012, **51**, 1387-1390.

19. S. Kelkar, C. M. Saffron, Z. Li, S.-S. Kim, T. J. Pinnavaia, D. J. Miller and R. Kriegel, *Green Chem.*, 2014, **16**, 803-812.

20. A. Veses, B. Puértolas, M. S. Callén and T. García, *Micropor. Mesopor. Mat.*, 2015, **209**, 189-196.

21. M. M. Yung, A. R. Stanton, K. Iisa, R. J. French, K. A. Orton and K. A. Magrini, *Energy & Fuels*, 2016, **30**, 9471-9479.

22. Y. Zheng, F. Wang, X. Yang, Y. Huang, C. Liu, Z. Zheng and J. Gu, *J. Anal. Appl. Pyrol.*, 2017, **126**, 169-179.

23. A. R. Stanton, K. Iisa, C. Mukarakate and M. R. Nimlos, *ACS Sust. Chem. Eng.*, 2018, **6**, 10030-10038.

24. J. Jae, R. Coolman, T. J. Mountziaris and G. W. Huber, *Chem. Eng. Sci.*, 2014, **108**, 33-46.

25. C. A. Mullen, P. C. Tarves, L. M. Raymundo, E. L. Schultz, A. A. Boateng and J. O. Trierweiler, *Energy & Fuels*, 2018, **32**, 1771-1778.

26. K. M. Dooley, C. Chang and G. L. Price, *Appl. Catal. A*, 1992, **84**, 17-30.

27. V. B. Kazansky, I. R. Subbotina, N. Rane, R. A. van Santen and E. J. Hensen, *Phys. Chem. Chem. Phys.*, 2005, **7**, 3088-3092.

28. E. Mansoor, M. Head-Gordon and A. T. Bell, *ACS Catal.*, 2018, **8**, 6146-6162.

29. M. W. Schreiber, C. P. Plaisance, M. Baumgärtl, K. Reuter, A. Jentys, R. Bermejo-Deval and J. A. Lercher, *J. Am. Chem. Soc.*, 2018, **140**, 4849-4859.

30. M. Niwa, K. Suzuki, N. Morishita, G. Sastre, K. Okumuraa and N. Katadaa, *Catal. Sci. Technol.*, 2013, **3**, 1919-1927.

31. P. Dumrongsakda and V. Ruangpornvisuti, *Catal. Lett.*, 2011, **142**, 143-149.

32. A. Heyden, B. Peters, A. T. Bell and F. J. Keil, *J. Phys. Chem. B*, 2005, **109**, 1857-1873.

33. A. L. Yakovlev, G. M. Zhidomirov and R. A. van Santen, *J. Phys. Chem. B*, 2001, **105**, 12297-12302.

34. C. Hammond, M. M. Forde, M. H. Ab Rahim, A. Thetford, Q. He, R. L. Jenkins, N. Dimitratos, J. A. Lopez-Sanchez, N. F. Dummer, D. M. Murphy, A. F. Carley, S. H. Taylor, D. J. Willock, E. E. Stangland, J. Kang, H. Hagen, C. J. Kiely and G. J. Hutchings, *Angewandte Chemie*, 2012, **51**, 5129-5133.

35. T. Maihom, P. Khongpracha, J. Sirijaraensre and J. Limtrakul, *ChemPhysChem*, 2013, **14**, 101-107.

36. C. Zhao, J. He, A. A. Lemonidou, X. Li and J. A. Lercher, *J. Catal.*, 2011, **280**, 8-16.

37. J. Sirijaraensre and J. Limtrakul, *Struc. Chem.*, 2012, **24**, 1307-1318.

38. J. A. Ryder, A. K. Chakraborty and A. T. Bell, *J. Phys. Chem. B*, 2002, **106**, 7059-7064.

39. M. F. Fellah and I. Onal, *Catal. Today*, 2008, **137**, 410-417.

40. M. J. Rice, A. K. Chakraborty and A. T. Bell, *J. Phys. Chem. A*, 1998, **102**, 7498-7504.

41. S. Yadnum, S. Choomwattana, P. Khongpracha, J. Sirijaraensre and J. Limtrakul, *ChemPhysChem*, 2013, **14**, 923-928.

42. J. S. Woertink, P. J. Smeets, M. H. Groothaert, M. A. Vance, B. F. Sels, R. A. Schoonheydt and E. I. Solomon, *Proc. Natl. Acad. Sci.*, 2009, **106**, 18908-18913.

43. A. L. Yakovlev, A. A. Shubin, G. M. Zhidomirov and R. A. van Santen, *Catal. Lett.*, 2000, **70**, 175-181.

44. J. Xu, A. Zheng, X. Wang, G. Qi, J. Su, J. Du, Z. Gan, J. Wu, W. Wang and F. Deng, *Chem. Sci.*, 2012, **3**, 2932-2940.

45. E. Pidko, V. Kazansky, E. Hensen and R. Vansanten, *J. Catal.*, 2006, **240**, 73-84.

46. Y. V. Joshi and K. T. Thomson, *Catal. Today*, 2005, **105**, 106-121.

47. Y. V. Joshi and K. T. Thomson, *J. Catal.*, 2007, **246**, 249-265.

48. M. S. Pereira and M. A. C. Nascimento, *J. Phys. Chem. B*, 2006, **110**, 3231-3238.

49. M. S. Pereira, A. M. da Silva and M. A. C. Nascimento, *J. Phys. Chem. C*, 2011, **115**, 10104-10113.

50. E. A. Pidko, E. J. M. Hansen and R. A. van Santen, *J. Phys. Chem. C*, 2007, **111**, 13068-13075.

51. G. M. Zhidomirov, A. A. Shubin, M. A. Milov, V. B. Kazansky, R. A. van Santen and

E. J. M. Hansen, *J. Phys. Chem. C*, 2008, **112**, 3321-3326.

52. I. V. Kuz'min, G. M. Zhidomirov, V. N. Solkan and V. B. Kazanskii, *Kinet. Catal.*, 2009, **50**, 752-759.

53. M. S. Stave and J. B. Nicholas, *J. Phys. Chem.*, 1995, **99**, 15046-15061.

54. N. O. Gonzales, A. K. Chakraborty and A. T. Bell, *Catal. Lett.*, 1998, **50**, 135-139.

55. V. B. Kazansky, I. R. Subbotina, R. A. van Santen and E. J. M. Hensen, *J. Catal.*, 2004, **227**, 263-269.

56. N. Rane, A. Overweg, V. Kazansky, R. Vansanten and E. Hensen, *J. Catal.*, 2006, **239**, 478-485.

57. A. B. Getsoian, U. Das, J. Camacho-Bunquin, G. Zhang, J. R. Gallagher, B. Hu, S. Cheah, J. A. Schaidle, D. A. Ruddy, J. E. Hensley, T. R. Krause, L. A. Curtiss, J. T. Miller and A. S. Hock, *Catal. Sci. Technol.*, 2016, **6**, 6339-6353.

58. N. M. Phadke, J. Van der Mynsbrugge, E. Mansoor, A. B. Getsoian, M. Head-Gordon and A. T. Bell, *ACS Catal.*, 2018, **8**, 6106-6126.

59. E. J. Hensen, E. A. Pidko, N. Rane and R. A. van Santen, *Angewandte Chemie*, 2007, **46**, 7273-7276.

60. H.-m. Chang, B. Cowling Ellis and W. Brown, *hfsg*, 1975, **29**, 153.

61. C. Freitas, N. S. Barrow and V. Zholobenko, *Johnson Matthey Technol. Rev.*, 2018, **62**, 279-290.

62. B. Ravel and M. Newville, *J. Synchrotron Radiat.*, 2005, **12**, 537-541.

63. M. Xu, C. Mukarakate, K. Iisa, S. Budhi, M. Menart, M. Davidson, D. J. Robichaud, M. R. Nimlos, B. G. Trewyn and R. M. Richards, *ACS Sust. Chem. Eng.*, 2017, **5**, 5477-5484.

64. K. Iisa, R. J. French, K. A. Orton, M. M. Yung, D. K. Johnson, J. ten Dam, M. J. Watson and M. R. Nimlos, *Energy & Fuels*, 2016, **30**, 2144-2157.

65. S. Dappricha, I. a. K.́aromia, K. S. Byuna, K. Morokumaa and M. J. Frisch, *J. Mol. Struc. (Theochem)*, 1999, **461-462**, 1-21.

66. Y. Zhao and D. G. Truhlar, *Theor. Chem. Acc.*, 2007, **120**, 215-241.

67. N. O. Gonzales, A. T. Bell and A. K. Chakraborty, *J. Phys. Chem. B*, 1997, **101**, 10058-10064.

68. S. Lonsinger, A. Chakraborty, D. Theodorou and A. T. Bell, *Catal. Lett.*, 1991, **11**, 209-217.

69. J. J. Stewart, *J. Mol. Model.*, 2007, **13**, 1173-1213.

70. S. Kim, D. J. Robichaud, G. T. Beckham, R. S. Paton and M. R. Nimlos, *J. Phys. Chem. A*, 2015, **119**, 3604-3614.

71. C. Gonzalez and H. B. Schlegel, *J. Phys. Chem.*, 1990, **94**, 5523-5527.

72. M. J. Frisch, G. W. Trucks, H. B. Schlegel, G. E. Scuseria, M. A. Robb, J. R. Cheeseman, G. Scalmani, V. Barone, G. A. Petersson, H. Nakatsuji, X. Li, M. Caricato, A. Marenich, J. Bloino, B. G. Janesko, R. Gomperts, B. Mennucci, H. P. Hratchian, J. V. Ortiz, A. F. Izmaylov, J. L. Sonnenberg, D. Williams-Young, F. Ding, F. Lipparini, F. Egidi, J. Goings, B. Peng, A. Petrone, T. Henderson, D. Ranasinghe, V. G. Zakrzewski, J. Gao, N. Rega, G. Zheng, W. Liang, M. Hada, M. Ehara, K. Toyota, R. Fukuda, J. Hasegawa, M. Ishida, T. Nakajima, Y. Honda, O. Kitao, H. Nakai, T. Vreven, K. Throssell, J. J. A. Montgomery, J. E. Peralta, F. Ogliaro, M. Bearpark, J. J. Heyd, E. Brothers, K. N. Kudin, V. N. Staroverov, T. Keith, R. Kobayashi, J. Normand, K. Raghavachari, A. Rendell, J. C. Burant, S. S. Iyengar, J. Tomasi, M. Cossi, J. M. Millam, M. Klene, C. Adamo, R. Cammi, J. W. Ochterski, R. L. Martin, K. Morokuma, O. Farkas, J. B. Foresman and D. J. Fox, *Gaussian 09*, Revision D.01, Gaussian, Inc., Wallingford CT, 2016.

73. I. Funes-Ardoiz and R. S. Paton, *GoodVibes*, 2017, DOI: 10.5281/zenodo.884527.

74. A. E. Reed, L. A. Curtiss and F. Weinhold, *Chem. Rev.*, 1988, **88**, 899-926.

75. G. A. Ferguson, V. Vorotnikov, N. Wunder, J. Clark, K. Gruchalla, T. Bartholomew, D. J. Robichaud and G. T. Beckham, *J. Phys. Chem. C*, 2016, **120**, 26249-26258.

76. T. R. Carlson, Y.-T. Cheng, J. Jae and G. W. Huber, *Energy Environ. Sci.*, 2011, **4**, 145-161.

77. C. Mukarakate, M. J. Watson, J. ten Dam, X. Baucherel, S. Budhi, M. M. Yung, H. Ben, K. Iisa, R. M. Baldwin and M. R. Nimlos, *Green Chem.*, 2014, **16**, 4891-4905.

78. D. Gao, C. Schweitzer, H. T. Hwang and A. Varma, *Ind. Eng. Chem. Res.*, 2014, **53**, 18658-18667.

79. H. M. Wang, J. Male and Y. Wang, *ACS Catal.*, 2013, **3**, 1047-1070.

80. A. Veses, B. Puértolas, J. M. López, M. S. Callén, B. Solsona and T. García, *ACS Sust. Chem. Eng.*, 2016, **4**, 1653-1660.

81. A. R. Stanton, K. Iisa, M. M. Yung and K. A. Magrini, *J. Anal. Appl. Pyrol.*, 2018, **135**, 199-208.

82. G. D. Meitzner, E. Iglesia, J. E. Baungartner and E. S. Huang, *J. Catal.*, 1993, **140**, 209-225.
83. K. Wang, P. A. Johnston and R. C. Brown, *Bioresource technology*, 2014, **173**, 124-131.
84. G. Luo and F. L. P. Resende, *Fuel*, 2016, **166**, 367-375.
85. S. Wan, C. Waters, A. Stevens, A. Gumidyala, R. Jentoft, L. Lobban, D. Resasco, R. Mallinson and S. Crossley, *ChemSusChem*, 2015, **8**, 552-559.
86. U. Olsbye, S. Svelle, M. Bjorgen, P. Beato, T. V. Janssens, F. Joensen, S. Bordiga and K. P. Lillerud, *Angewandte Chemie*, 2012, **51**, 5810-5831.
87. L. Y. Jia, M. Raad, S. Hamieh, J. Toufaily, T. Hamieh, M. M. Bettahar, G. Mauviel, M. Tarrighi, L. Pinard and A. Dufour, *Green Chem.*, 2017, **19**, 5442-5459.
88. T. P. Vispute, H. Zhang, A. Sanna, R. Xiao and G. W. Huber, *Science*, 2010, **330**, 1222-1227.
89. W. Wang and M. Hunger, *Acc. Chem. Res.*, 2008, **41**, 895-904.